Korean J. Chem. Eng., 39(3), 616-627 (2022)
DOI: 10.1007/s11814-021-0952-8

pISSN: 0256-1115
eISSN: 1975-7220

Fabrication of modified nanofiltration membranes by functionalized cellulose nanocrystals with high anti-fouling capability in removing dye from water and wastewater

Mozhdeh Amiri, Ehsan Jafarbeigi, and Farhad Salimi†

Department of Chemical Engineering, Kermanshah Branch, Islamic Azad University, Kermanshah, Iran
(*Received 27 April 2021 • Revised 31 August 2021 • Accepted 5 September 2021*)

Abstract−The aim of this study was to remove Azo dye, Direct Red 16, from a synthetic solution, 50 mg/l, and also to treat the wastewater of the licorice extract plant, LEP, by nanofiltration membrane with high anti-fouling properties. In this regard, a new polymer nanocomposite was fabricated by mixing cellulose nanocrystals functionalized with amino acid cysteine (CNF-AAC) and investigating the effective parameters such as anti-fouling properties, as well as the performance of the modified membrane in removing the dye. In this regard, field emission scanning electron microscopy (FESEM), scanning-force microscopy (SFM), atomic force microscopy (AFM) and contact angle measurements were performed. The results of AFM analysis indicated that the surface roughness of polyether sulfone-membrane is reduced by the addition of CNF-AAC. Therefore, by increasing the concentration of nanocrystals from 0 to 1 wt% in the initial solution of the membrane, the net distilled water flux permeation has increased from 18.05 (kg/m^2h) to 26.50 (kg/m^2h). Also, with increasing the concentration of CNF-AAC in the initial solution of the membranes, the size of the contact angle has gradually decreased. Meanwhile, adding a small amount of CNF-AAC (0.5 wt%) to the polyether-sulfone membrane has led to reducing the rate of irreversible fouling from 43.34% to 4.89% and in contrast, to increasing the amount of reversible fouling from 30.02% to 63.54%. On the other hand, in this study, the yield of dye solution by the optimal membrane is 98.38%, for which the percentage of COD removal for the wastewater of LEP has reached 90%.

Keywords: Nanofiltration, Licorice Extract Factory Wastewater, Cellulose Nanocrystals Functionalized with the Amino Acid Cysteine, Polyether-sulfone, Direct Red 16

INTRODUCTION

Organic pollutants are the most important sources of environmental pollution that have a very dangerous effect on the environment, human health and especially water resources. These pollutants are very stable and do not disappear easily in nature, so it is necessary to remove them from the environment in some way [1]. One of these organic pollutants is synthetic dyes, which have a significant presence in our lives today and their use is constantly increasing [2]. It is necessary to mention that today about 26,000 types of dyes are produced worldwide. Many countries have imposed environmental regulations due to the adverse effects of these pollutants, including the need to decolorize dye wastewaters before discharging them into the environment. However, more than one million tons of dyes are produced annually, of which, 280,000 tons of dyes are discharged directly into wastewater [3]. One of the most important and useful dyes of azo is direct red dye 16. This dye is reported to be highly carcinogenic, mutagenic and resistant to biological degradation [4]. Therefore, an efficient technique should be devised to remove DR16 from water and wastewater.

Many methods, such as biological, oxidation or ozonation [5,6], flocculation [7], adsorption [8,9], have been tested with the aim of removing dye from industrial wastewater. However, most of these methods have disadvantages such as inability to degrade dyes and produce toxic by-products [10-12]. Given the above about the dangers of dye entering water sources, we need to choose an appropriate method to effectively remove dye from water. According to research, one of the most suitable methods to remove dye from water is nanofiltration membrane technology [13]. Membrane processes can be introduced as one of the effective and efficient processes for dye removal [14,15].

Membrane filtration technology with different types of membranes has appeared in the separation process of organic pollutants due to its high efficiency, ease of management and space-savings. Membrane technologies for the removal of pollutants from wastewater include microfiltration, ultrafiltration, nanofiltration, reverse osmosis, electrodialysis, which are widely used in various industries today [16]. To get the best performance by separation, nanofiltration (NF) membranes seem to be effective due to their nanoporous structure that most of organic matters cannot pass through these nanopores. Madaeni et al. evaluated the separation of liquidity from glycyrrhizic acid in licorice root extract using nanofiltration (NF) polymer membrane (NRT-7450 from Hydranautics) and a molecular weight cut off (MWCO) in the range of 600-700 [17]. In this regard, a process of separation of glycyrrhizic acid from licorice root extract based on the use of ultrafiltration (UF) membranes was also patented by Gorgol et al. [18].

One of the most advanced membrane materials containing nano-

†To whom correspondence should be addressed.
E-mail: f.salimi@iauksh.ac.ir

materials in its polymer matrix is the nanocomposite membrane that can be used to separate gas - gas, liquid - liquid, liquid - solid separation. Due to their promise to resolve the exchange relationship between selectivity and permeability as well as reducing the problem of membrane deposit during purification of water, has gained increasing attention and is considered to be cut-through next generation of membrane with high performance [19,20].

In recent decades, membrane treatment technologies in the water and wastewater treatment industry have increasingly shown acceptable performance in the work process. So, it can be said that those have more significant advantages over traditional methods [21]. One of the suitable candidates for this purpose is cellulosic nanocrystals (CNC). These materials are used because of many benefits like renewability, biodegradability, environmental instability and appropriate thermal stability [22]. In addition, the CNC has a surface that is easy to operate and allows the incorporation of chemical moieties and increases the binding efficiency of contaminants to the modified CNC. Rafieian et al. developed membranes based on polyethersulfone (PES) as matrix and amine functionalized cellulose nanocrystals as nanofiller for copper ion and direct red-16 removal from water. CNC surface modification was performed using (3 - aminopropyl) triethoxysilane. The results showed that the maximum adsorption capacity of copper ion and dye removal was 90% and 99%, respectively, for the membranes [23]. In another work, cellulose acetate (CA) was used to provide specific structures and cavities for membrane applications, and the results showed that the ability of the membranes increased in the rejection of the water microorganisms [24]. Bai et al. showed that TEMPO oxidized cellulose nanocrystals with negative functional groups can be used to functionalize electrospun membranes, which provides a route to reject bacteria via size exclusion and reject virus via adsorption [23].

In this study, synthesized hydrophilic membranes with high anti-fouling ability were used to remove dyes (Direct red 16) and to treat the wastewater of LEP. Also, to solve the membrane fouling problem, cellulose nanocrystals were functionalized with the amino acid cysteine to reduce membrane fouling and increase the output flux and absorption of pollutants. Parameters affecting the performance of nanocomposite materials such as anti-fouling properties, modified membrane performance were studied in removing the dye and reduction of wastewater load and the calculation of flux recovery ratio. Also, to better analyze the results of the prepared membrane, SEM, FTIR, AFM, AFM, and measurement of water contact angle were used. Innovation done in this work is the synthesis and application of new polymer nanocomposite as a multifaceted combination agent to reduce the contact angle simultaneously in order to remove Azo dye and treat wastewater of LEP.

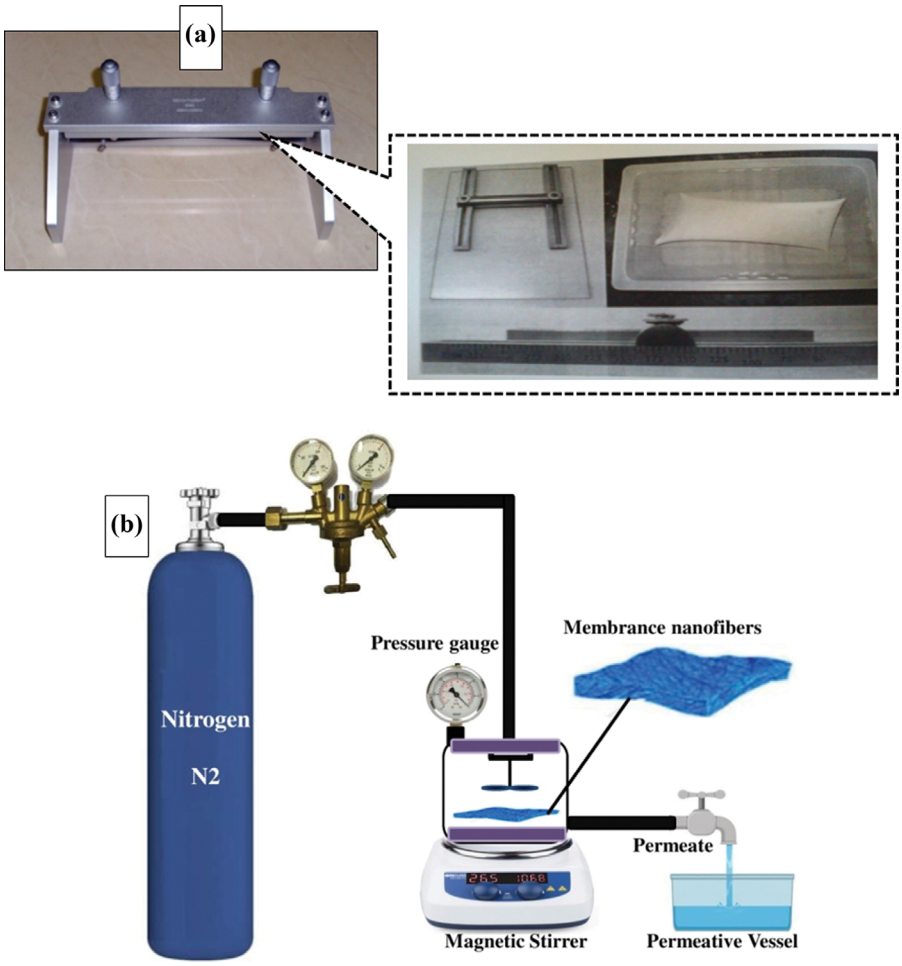

Fig. 1. (a) Used elcometer stretch film, (b) The dead-end membrane system used in experiments.

EXPERIMENTAL SET-UP AND METHODOLOGY

1. Materials

In this research, in order to make nanofiltration membranes, Ultrason S PES, E6020 P grade polyether-sulfone chemicals from German company BASF, Dimethylacetamide solvent (DMAc) from German company Merck and Polyvinylpyrrolidone polymer with an average molecular weight of 29,000 $g \cdot mol^{-1}$ from Sigma company were used. Also, Elcometer 3580 stretch film with 15 cm wide was used to make the membranes which are shown in Fig. 1(a). Also to fabricate the functionalized cellulose nanocrystals, cellulose nanocrystals from Merck company, cysteine amino acid manufactured by Merck company with a molecular mass of 121.15 $g \cdot mol^{-1}$, ethanol manufactured by Merck company with a molar mass of 46.07 $g \cdot mol^{-1}$ volumetric mass 0.789 $kg \cdot L^{-1}$ at a temperature of 25 °C and glacial acetic acid made by Merck company with a mass of 60.05 $g \cdot mol^{-1}$, a volume mass of 1.05 $kg \cdot L^{-1}$ at 20 °C and purity of over 99.8% have been used. The azo dye, direct red 16, $C_{26}H_{17}N_5Na_2O_8S_2$ (C.I. 27680, MW 637.26) was purchased from Alvan Sabet company, 99% pure.

2. Equipment

Equipment used in this research includes: Sonopuls model ultrasonic device from Bandelin company, convection oven NDO-400 model from Eyela company, 5,000 rpm centrifugal device Hettich model made in Germany, RKB2 styler from IKA company, Shimadzu Electronic Balances, Lambda2S UV-Vis spectrometer from Perkin Elmer company, Philips X'Pert-MPD X-ray diffraction device, Philips XL-30ESM scanning electron microscope (SEM), Fourier transform infrared spectroscopy (FT-IR) Nicolet MagnaIR 550 model and Atomic force microscope (AFM) Dual Scope (DME model C-21).

3. Membrane Fabrication

3-1. Synthesis of CNF-AAC

Initially, 1 g of cellulose nanocrystals was added to 50 ml of ethanol and the solution was vigorously mixed in a three-portion balloon on a magnetic stirrer. Then 5 ml of ethanol solution with 10 mM amino acid cysteine in 50 ml of ethanol was mixed dropwise and added to the cellulose nanocrystal solution under severe stirring conditions. At this stage, the pH of the solution was adjusted to about 3 to 4 by adding concentrated HCl (12 M) drop by drop. Finally, the solution was refluxed for 60 hours at 60 °C. The precipitate from the functionalization process was washed several times with ethanol and distilled water and dried at 105 °C for 15 minutes.

3-2. Fabrication of Sulfone Polyether Membrane Modified with CNF-AAC

In this study, the rapid phase transition (RPT) method was used to make pure and composite membranes. In the fabrication of all these membranes, 20 wt% of polyether-sulfone (PES) and 1 wt% of Polyvinylpyrrolidone (PVP) (to increase the cavities in the settling stage) were used as in Table 1. In the fabrication stage of composite membranes, with the aim of homogenization, the solution containing nanocrystals and solvent was first placed in an ultrasonic bath for 30 minutes. Then PES and PVP were added and the whole solution was mixed for 24 hours by a magnetic stirrer at a speed of 400 rpm at 28 °C until completely uniform. Finally, to better disperse the nanocrystals in the polyether-sulfone solution and also to remove the trapped air bubbles, the solution was placed in a supernatant bath for 30 minutes. In the last step, the solution was fixed on a completely clean and clean glass using a blade and stretched to a thickness of 150 μm. The glass was then rapidly immersed in a gelation bath containing a non-solvent polymer (water) at 20 °C to form a precipitated polymer and an asymmetric porous membrane by the phase transition and solvent exiting. The prepared membranes were immersed in fresh distilled water for 24 hours to complete phase transition and PVP exiting. Finally, the membranes were placed between two filter papers for 24 hours to dry at room temperature [25,26].

Table 1. Combining the percentage of synthesized polyether-sulfone membranes with different weight percentages of CNF-AAC

Membrane type	PES (wt%)	PVP (wt%)	Nanocrytalline cellulose (wt%)
M_1	20	1	0
M_2	20	1	0.1
M_3	20	1	0.5
M_4	20	1	1

3-3. Characteristics of Modified Cellulose Nanocrystals and Prepared Membranes

FT-IR spectroscopy was used to prove the presence of the functional group in cellulose nanocrystals. To perform this test, cellulose nanocrystals were first placed on KBr tablets and then examined by FT-IR. The surface morphology of the synthesized cellulose nanocrystals was also examined by scanning electron microscopy. On the other hand, Sessile drop method was used to measure the contact angle of the membrane. Larger contact angles indicate more hydrophobicity for the membrane surface, while hydrophilic surfaces have lower contact angles. The samples were then cut into 2 cm×24 cm sizes and washed with distilled water. These samples were glued to a black holder. Here, double distilled water was used as the column fluid in contact angle experiments. To minimize measurement error, contact angles were measured at five different locations in the sample and their mean was reported as the final contact angle. A scanning electron microscope was used to examine the cross-section structure of the membranes. The use of atomic electron microscopy has high efficiency for accurate analysis of morphology and surface roughness. In addition to calculating the roughness of the membrane surface, the size of the membrane surface pores can also be obtained by using AFM software and AFM images simultaneously. Here, to take AFM images, the membranes were cut to 1 cm×1 cm and glued in a special place. Finally, the surface of the membranes was photographed at different scan sizes such as 1 μm×1 μm and 2 μm×2 μm. The device used in this project was Dual Scope (DME model C-21).

4. Experimental Set-up

To test the fabricated membranes, a dead-end cell was used according to Fig. 1(b). In this regard, the membranes were cut into an effective diameter of 5 cm and placed in the cell. Nitrogen gas was also used to provide the driving force in this system. The performance of the fabricated nanofiltration membranes was evaluated in terms of feed output flux and removal percentage using Direct Red 16 dye with a concentration of 50 ppm and distilled

Table 2. Characteristics of licorice factory wastewater

Wastewater	Parameter	Amount	Unit
Licorice root extract wastewater	TS	1,680	ppm
	TDS	1,520	ppm
	COD	813	mg/L
	Turbidity	37.8	NTU
	pH	8.2	-

water after permeability testing of the membranes for 60 minutes. The dye removal percentage was calculated according to Eq. (1) [14]. The wastewater treatment characteristics of the studied LEP wastewater are described in Table 2.

$$\% \text{ Rejection} = \left(1 - \frac{C_p}{C_F}\right) \times 100 \quad (1)$$

Here C_p and C_F are Direct Red 16 dye concentrations in the product and feed, respectively.

The removal percentage of COD was calculated according to Eq. (1), where C_p and C_F are the COD concentration of the wastewater in the product and feed, respectively.

5. Fouling Test and Calculation of Anti-fouling Property

The amount of solvent passing through the membranes under applied pressure within a fixed time interval was used to calculate water flux ($Lm^{-2}h^{-1}MPa^{-1}$). The water flux (F) was calculated using Eq. (2).

$$F = \frac{V_0(L)}{T_0(h)} \times A_0(m^2) \times P_0(MPa) \quad (2)$$

where V_0 is volume of solvent that passed through the membrane, T_0 is time of measurement, A_0 is effective membrane area and P_0 is applied pressure.

Milk Powder feed with a concentration of 8,000 ppm was used to evaluate the anti-fouling properties immediately after distilled water permeability test. The high concentration of Milk Powder allows handling high and acceptable fouling in 2 hours. Here, after the distilled water permeability test (for 120 minutes), the output flux for milk powder J_p kg/(m^2·h) was measured at 5 bar pressure for 2 hours. The membranes used in the previous step were immersed in distilled water (without any cleaning agent) for 30 minutes, and after rinsing with water, the outlet flux of distilled water was measured after fouling J_{w2} kg/(m^2·h) (Within 2 hours to reach a fixed value) [27].

To measure the resistance to fouling, the flux recovery ratio (FFR) parameter was calculated using Eq. (3), the highest value of which indicates better anti-fouling properties [28]:

$$\text{Flux Recovery ratio} = \frac{J_{wp,2}}{J_{wp,1}} \times 100 \quad (3)$$

Here $J_{wp,2}$ is the pure water flux after filtration and $J_{wp,1}$ is the pure water flux before filtration. Fouling process analysis was examined more accurately by various parameters to better describe the anti-fouling capability of composite membranes.

Thus, the total resistance to crossing the flow that occurs during the filtration process indicates fouling of the membrane, which is determined by Eq. (4) [29]:

$$R_t = \left(1 - \frac{j_p}{j_{w,1}}\right) \times 100 \quad (4)$$

Here R_t (percentage of total fouling) indicates a decrease in total flux due to total fouling. Also, in Eq. (5) and (6), R_r and R_{ir}, respectively, are often expressed to indicate reversible fouling ratio and irreversible fouling ratio. The percentage of reversible fouling describes the fouling due to concentration polarization; on other hand, the percentage of irreversible fouling indicates fouling due to adsorption or deposition of protein molecules on the membrane surface [30].

$$R_r = \left(\frac{J_{w2} - J_p}{J_{w1}}\right) \times 100 \quad (5)$$

$$R_{ir} = \left(\frac{J_{w1} - J_{w2}}{J_{w1}}\right) \times 100 \quad (6)$$

It is clear that R_t is the sum of R_{ir} and R_r. These parameters help to better understand the behavior of the membrane in the fouling process. Lower total fouling and higher reversible fouling indicate better membrane performance in fouling reuse.

RESULTS AND DISCUSSION

1. Identification of CNF-AAC

The FT-IR spectrum, XRD spectrum and FE-SEM images of the synthesized cellulose nanocrystals are shown in Fig. 2. In this study, the FT-IR pattern of the modified cellulose nanocrystals is illustrated in Fig. 2(a). The modified FTIR nanocrystalline spectrum shows a large bond in the range of 3,200 cm^{-1} to 3,500 cm^{-1}, which is related to the stretching vibrations of the OH group in cellulose molecules. Also, in the modified FT-IR spectra of nanocrystals, CN stretching vibrations are observed around 2,061 cm^{-1}. The peak at 1,559 cm^{-1} resulting from the NH bending vibration indicates the presence of the amino acid cysteine group on the surface of cellulose nanocrystals. The peak at 3,087 cm^{-1} is also related to the stretching vibrations of the NH and OH groups [31,32]. The spectrum of X-ray diffraction test of the CNF-AAC is shown in Fig. 2(b). Three obvious peaks can be seen in 2θ=14.77, 16.5, 22.7, which represent the monoclinic crystal plates (101), (102) and (002), respectively. Also, the depression of 2θ=18 is due to the nanocrystalline cellulose amorphous region, which has more activity in the crystallization region [33]. On the other hand, Fig. 2(c), (d) shows the FE-SEM images for the synthesized crystals. As one can see in the picture, the nanocrystals are almost spherical with lumps. Also, according to the images, the average size of these nanocrystals is 23.5 nm. Also, Fig. 2(c), (d) shows the FE-SEM image of the modified nanocrystalline in which the textures are obvious at 100 nm and 200 nm.

2. Identification of Synthesized Membranes

2-1. Distilled Water Flux of Synthesized Membranes

The effect of the concentration of functionalized nanocrystals on the distilled water flux is shown in Fig. 3. By adding functionalized nanocrystals 0.5 wt% to the initial solution, the distilled water flux of the membrane increased from 18.05 kg/(m^2/hr) to 26.50

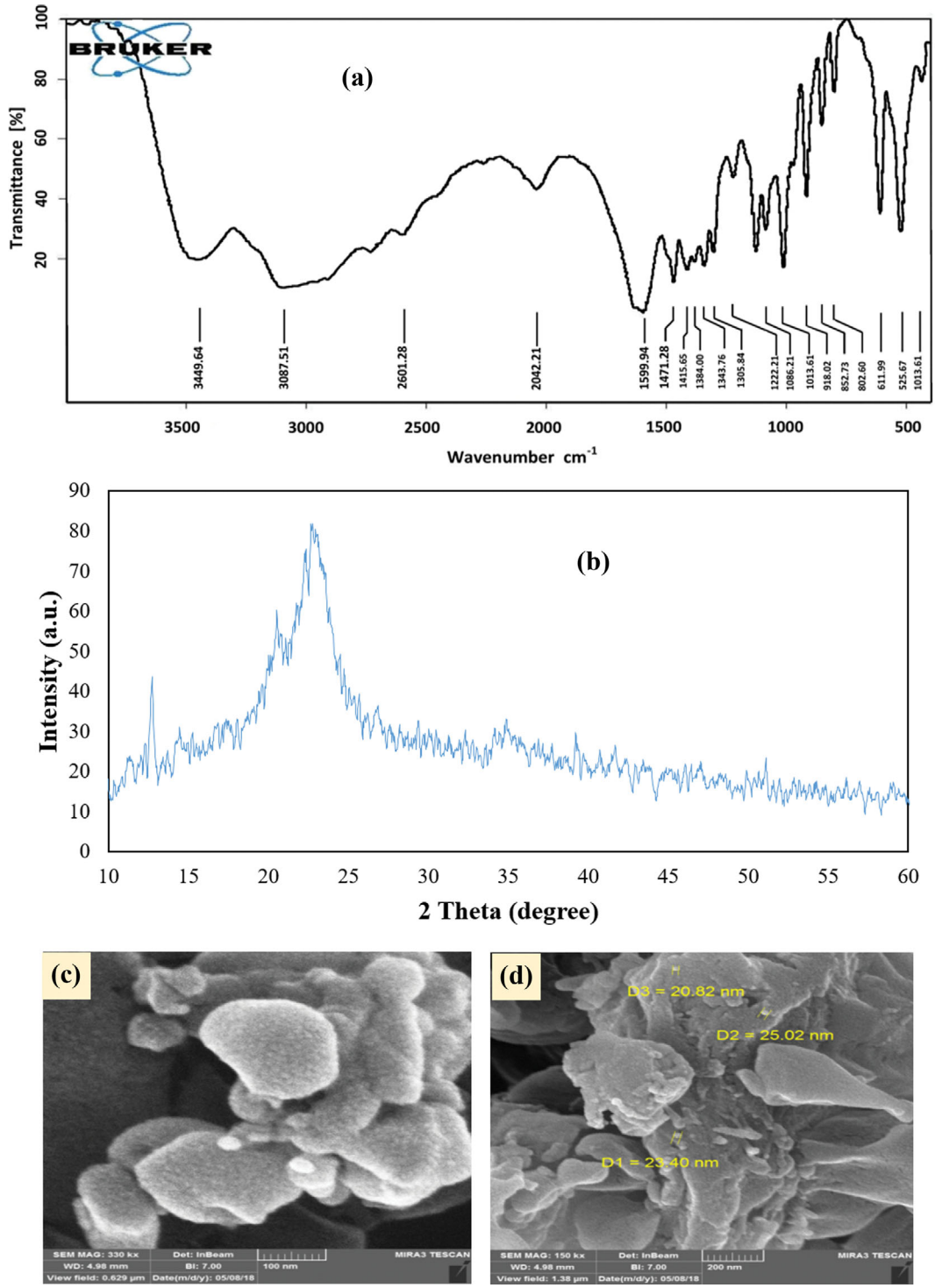

Fig. 2. (a) FT-IR spectrum, (b) XRD spectrum and (c), (d) FE-SEM image of functionalized cellulose nanocrystals at different magnifications.

kg/(m^2/hr). Then, by adding Larger amounts of nanocrystals in the distilled solution of the distilled water flux of the membrane changed from 26.50 kg/(m^2/hr) to 20.34 kg/(m^2/hr). Therefore, according to Fig. 3, it can be concluded that the addition of these nanocrystals caused a further increase in the flux of the modified membranes than the pure membrane. Also, the modified membrane M_3 with 0.5 wt% had the best permeability among the membranes produced. Increasing the concentration of nanocrystals in these membranes leads to increased porosity. Therefore, increasing the porosity leads to a decrease in water flow resistance and ultimately increased permeability of the membrane. Adding hydrophilic nanocrystals to the initial solution also improves hydrophilicity and increases the flux of pure water [34,35]. By increasing the concentration of nanocrystals to more than 0.5 wt%, their adhesion

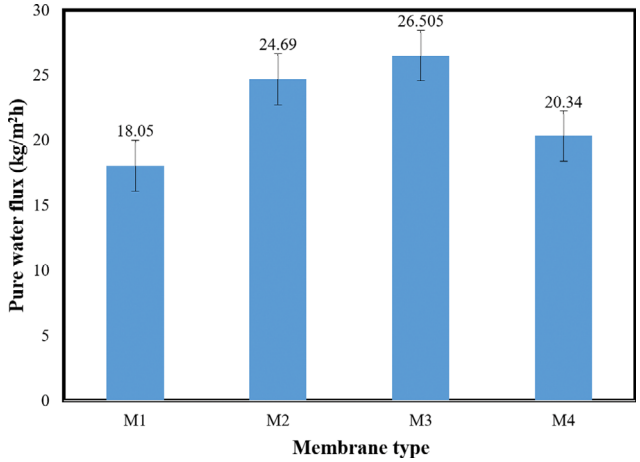

Fig. 3. Permeation flux through synthesized membranes with different percentages of CNF-AAC.

increases and then the viscosity of the polymer solution goes high. As a result, the rate of solvent and anti-solvent exchange in the gelation bath is reduced and the desired effect of using nanoparticles is not observed.

Also, increasing the concentration of nanoparticles in the initial solution of the membrane increases the viscosity of the solution. Due to this increase in viscosity, solvent (DMAc) and anti-solvent (water) displacement are more delayed during the fabrication of the membrane by the phase inversion method in the gelation bath, and as a result, the formation of larger diameter pores in the membrane structure, especially in the effective layer of the membrane surface is stopped. This phenomenon further reduces the permeation flux through (M_4) membrane compared to the (M_3) membrane [34].

2-2. Water Contact Angle and Effluent Turbidity

The contact angle values for pure and modified polyether-sulfone membranes and amino cysteine-functionalized nanocrystals are shown in Fig. 4. Examination of the results of contact angle measurements shows that with increasing the concentration of

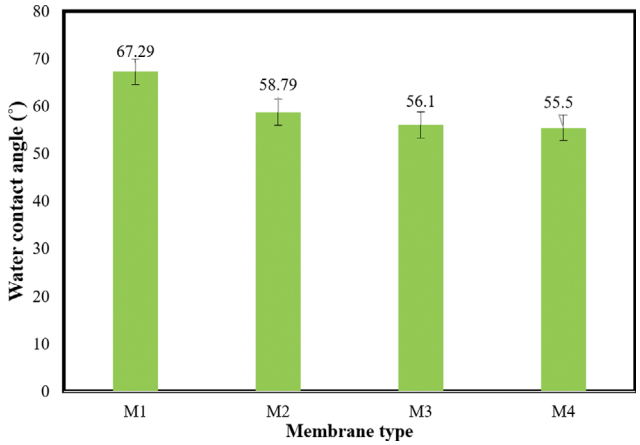

Fig. 4. Contact angle of synthesized membranes with different percentages of CNF-AAC.

nanocrystals in polyether-sulfone membranes, the contact angle decreases from 67.29 to 55.5 degrees. This is due to the high affinity of CNF-AAC on the surface of the membrane for water. As reported, the contact angle is inversely related to membrane hydrophilicity. That is, membranes made of different concentrations of nanocrystals in the initial solution have more hydrophilicity than pure polyether-sulfone membranes. Since the hydrophilicity of the modified membranes is higher, it is expected that their performance in terms of flux is higher than that of the pure polyether-sulfone membrane, which was also observed in the distilled water flux test [34,36]. Another reason for the decrease in the contact angle of the membranes and the increase in the hydrophilicity of their surface is the migration of hydrophilic nanoparticles to the joint surface of the membrane and water during the construction of the membrane by the phase inversion process in the gelation bath. This migration causes hydrophilic groups to be located on the upper surface of the membrane and increases the hydrophilicity of this surface. Many similar behaviors of different nanoparticles have been reported during membrane fabrication by the phase inversion process [34,37].

2-3. FE-SEM

The effect of functionalized nanocrystals on the morphology and performance of polyether-sulfone membranes can be explained as follows: Because the tendency between nanocrystals and water (non-solvent) is greater than that of polyether-sulfone, the time required to exchange between non-solvent (in the immersion bath) and solvent (from the film prepared from the mold solution) before gelation and vitrification, for solutions obtained from a mixture of nanocrystals and polyether-sulfone is more than polyether-sulfone. Longer exchange time between solvent and non-solvent in the gelation bath leads to further growth of the polymer droplet phase, in which case the lower layer of the membrane has larger pores and the upper surface of the membrane has a thinner and denser layer. Therefore, the density and pore size of nanocrystalline-modified membranes should be higher than the original polyether-sulfone membrane [25].

Fig. 5 shows that the addition of nanocrystals in the polymer solution changed the phase separation rate and led to a change in membrane structure. As shown in Fig. 5(a)-(d), all membranes are almost identically structured, as a dense initial layer is placed at the surface of the membrane and porous and finger-like cavities are also located at the bottom. It can also be seen from FESEM images that the addition of nanocrystals leads to creating a sublayer of the membrane with wider and larger finger-like cavities as well as higher porosity than pure polyether-sulfone membranes [30].

As mentioned in the previous section, increasing the concentration of cellulose nanocrystals by more than 0.5 wt% causes adhesion in them, increases the viscosity of the polymer solution and thus reduces the rate of solvent and anti-solvent exchange in the gelation bath. Therefore, the desired effect of the use of nanoparticles is not observed. The adhesion of nanocrystals in FESEM images of the cross-section of the membrane is shown in Fig. 5, which is evidence of this [30].

2-4. Atomic Electron Microscope (AFM)

Atomic electron microscope (AFM) images of membranes made with different weight percentages of CNF-AAC are shown in Fig. 6(a)-(d), respectively. In the pictures, the bright areas represent the

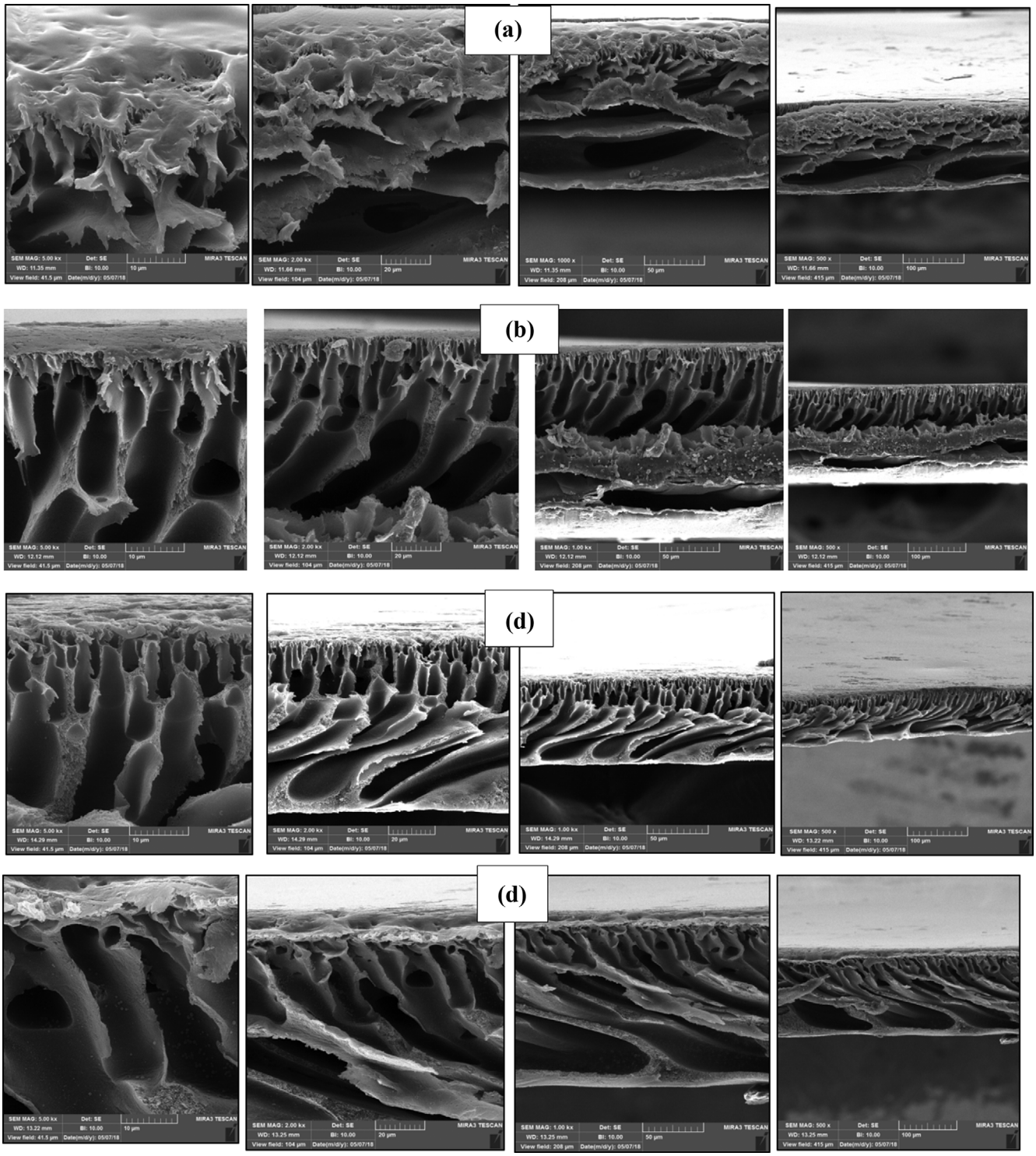

Fig. 5. FESEM images of the cross-section surface of a membrane made with different weight percentages of CNF-AAC. (a) Pure membrane, (b) 0.1 wt% CNF-AAC membrane, (c) 0.5 wt% CNF-AAC membrane, (d) 1 wt% CNF-AAC membrane.

high points and the dark areas represent the dimples or cavities of the membrane. It is clear from the AFM images that the structure of the polyether-sulfone membrane has undergone drastic changes due to the addition of hydrophilic nanocrystals to the initial polymer solution. The surface roughness parameters obtained from AFM images for nanoparticle-modified membranes are summarized in Table 3. Research has shown that the degree of membrane fouling decreases with decreasing surface roughness and also the membrane water content increases with decreasing roughness [38]. This phenomenon can be explained based on the casting cavity model. In this model, the size of the membrane cavities is equal to the empty space within the network of these protrusions. When

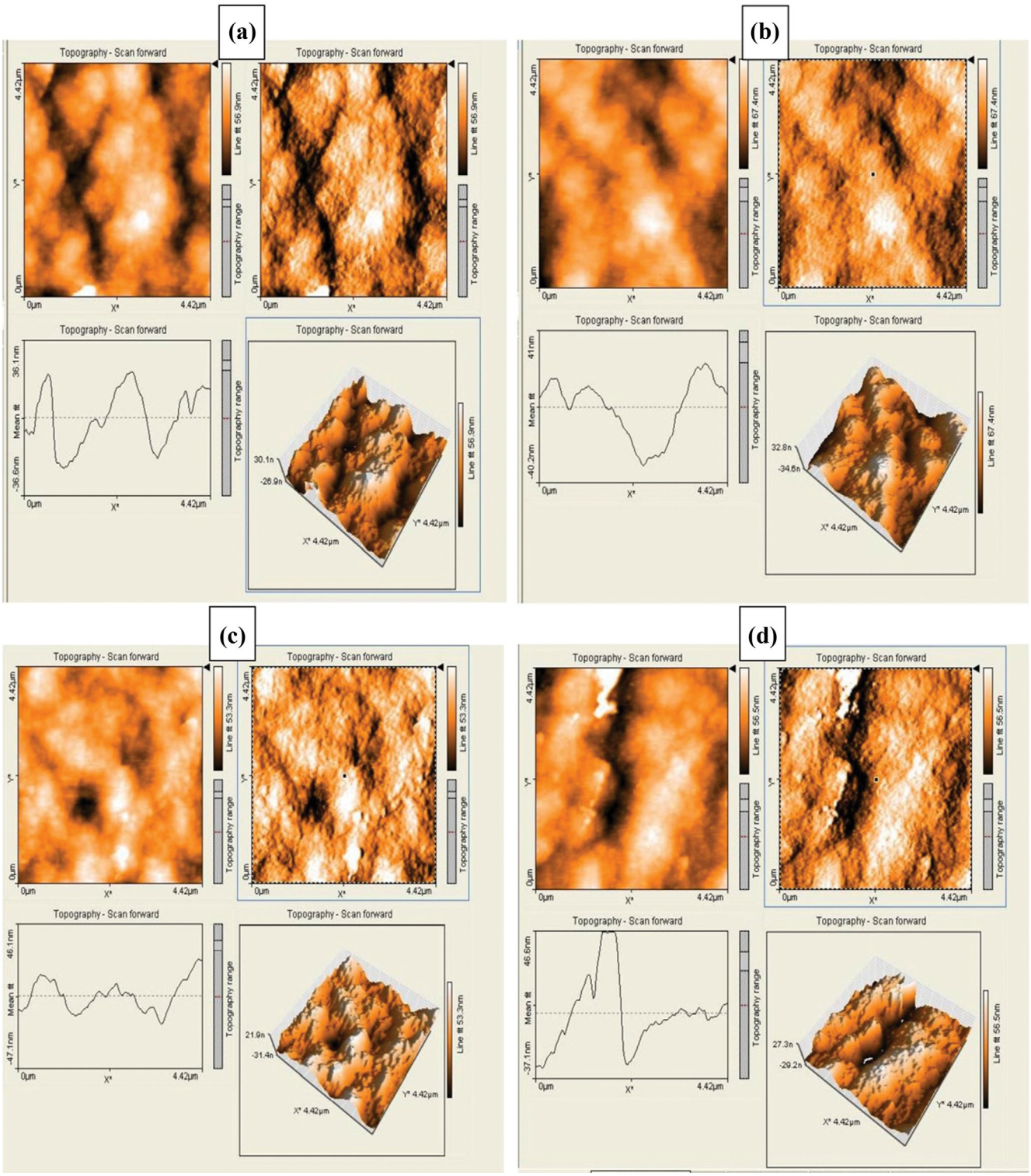

Fig. 6. AFM images of modified membranes with CNF-AAC. (a) Pure membrane, (b) 0.1 wt% CNF-AAC membrane, (c) 0.5 wt% CNF-AAC membrane, (d) 1 wt% CNF-AAC membrane.

these spherical protrusions are compressed on the surface of the membrane, the empty space between the protrusions is reduced, which increases the reparability of the membrane. On the other hand, if the protrusions are compressed, the depth of the gaps created between them is reduced, which means that smooth surfaces are created for the membrane. Therefore, on smooth surfaces, the gap between the protrusions is reduced, which increases the rate of salt or protein rejection. In addition, on smooth surfaces, the membrane surface fouling parameters are modified. So that a large amount of fouling agents and organic materials can easily be placed

Table 3. Surface roughness parameters for fabricated membranes

Membrane	Sa (nm)	Sq (nm)	Sz (nm)
M_1	73.56	95.48	1,167
M_2	10.226	12.52	83.208
M_3	7.289	9.195	69.819
M_4	9.998	12.637	96.79

in the empty space between the protrusions of rough surfaces and not get out of there in any way. In this case, irreversible membrane fouling occurs. This phenomenon occurs less on smooth surfaces due to the small space between the protrusions [38]. Roughness parameters include roughness average (Sa), root mean square of data; Z (Sq), an average of the height difference between highest peaks and the lowest valleys (Sz), which is obtained by analyzing AFM images. As shown in Fig. 6 and Table 3, the surface roughness of the polyether-sulfone membrane was reduced by the addition of nanoparticles. According to Table 3, the surface roughness parameters for the membrane modified by 0.5 wt% nanoparticles have the lowest value but, nevertheless, the surface roughness parameters in the membranes modified by weight percentages higher than 0.5 wt% are lower compared to the pure polyether-sulfone membrane. As mentioned, the reduction in surface roughness is probably due to the formation of a hydrogen bond between the polyether-sulfone layer and the groups present on the nanoparticle surface. Reduction of surface roughness can severely affect the adsorption properties of the membrane surface and fouling. Given the numerous sources, it has been proven that the smoother the surface of the membrane (less roughness), the greater its anti-fouling ability. Accumulation of pollutants and fouling agents in the surface roughness of the membrane may lead to an increase in its tendency to fouling.

3. Evaluation of Anti-fouling Properties of Synthesized Membranes

To evaluate the anti-fouling properties of the fabricated membranes, intermittent filtration experiments were performed using powdered milk solution (8,000 mg/L) as a suitable feed to evaluate membrane fouling. In each period of intermittent filtration experiments for each membrane, three phases are observed. The initial 60-minute interval in the diagram is related to the water permeation flux through the membranes. The second 90-minute interval is related to the dry milk solution permeation flux through the membrane, and finally, the third 60 minutes interval is related to the water the permeation flux through the membrane after 30 minutes of washing the membranes with distilled water Fig. 7(a).

Due to the strong stirring of the feed by the magnetic stirrer in the cell used for the experiments, the effect of concentration polarization on the membranes fouling can be ignored. Therefore, it can be said that the reduction of the permeation flux through the membranes is related to the materials that cause fouling on the membrane surface or sedimentation on the surface of the membranes. Also due to the irreversible surface adsorption caused by some of the fouling molecules caused by their entrapment in the pores of the membrane structure or their deposition on the membrane surface, the permeation flux through the membrane can never return

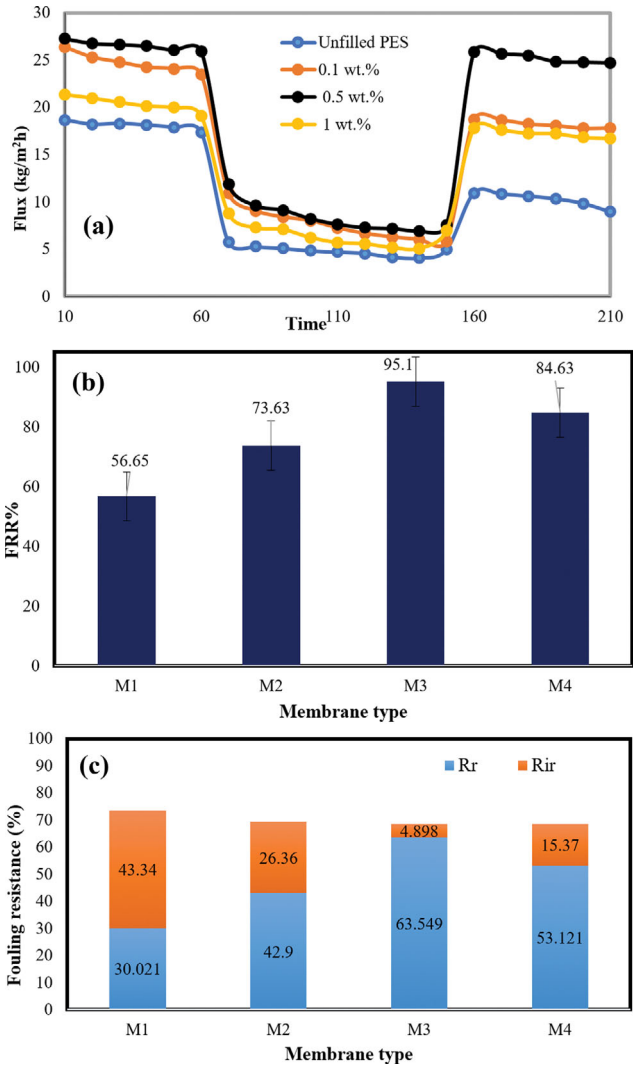

Fig. 7. (a) Anti-fouling performance, (b) Flux recovery ratio (c) and fouling parameters, of modified membranes with different weight percentages of CNF-AAC.

to its original level (water permeation flux in the initial 60-minute interval) after the third 60 minutes interval and after washing the membranes with distilled water. This phenomenon is shown by measuring the water flux recovery ratio (FRR) in Fig. 7(b). Fig. 7(b) shows the water FFR after fouling the surface of membranes with powder milk solution. Fig. 7(b) shows the FRR of the synthesized nanoparticle-modified membranes by weight percentages of 0-1. According to the results, the FRR for nanocrystals modified-membranes is higher than unmodified membrane. Also, the highest value of this parameter is 95.1%, which is related to the nanocrystals by weight percentage of 0.5 wt%. Higher FRR indicates a greater ability of the membrane to withstand fouling. As shown in Fig. 7(b), polyether-sulfone membrane (S_1) has the lowest recovery flux ratio (65.56%), which is due to the high hydrophobicity of the membrane surface, while the recovery flux ratio is significantly increased by adding nanocrystals to the membrane. The reason for this increase is the addition of hydrophilic functional groups to the membrane surface and the increase in hydrophilicity in the effective

layer of the membrane surface. The formation of hydrogen bonds between functional groups stretched across the membrane surface and water molecules creates a thin aqueous layer on the membrane surface, which is an effective factor in keeping fouling agents away from the membrane surface and leads to an increase in the recovery flux ratio. To more accurately survey the phenomenon of fouling in fabricated membranes, the resistance to reversible fouling (R_r) and irreversible fouling (R_{ir}) for fabricated membranes was calculated and the results are shown in Fig. 7(c). The results show that by adding a few nanoparticles (0.5 wt%) to the polyether-sulfone membrane, the rate of irreversible fouling has decreased from 43.34% to 4.89% and in contrast, the amount of reversible fouling has increased from 30.02% to 63.54%. The reason for this trend is less hydrophilicity and more non-uniformity of the surface of polyether-sulfone membranes than M_1 membrane, and also indicates that the modified membranes perform better in removing surface sediments when washed with water. Fig. 7(c) shows the fouling parameters for the synthesized membranes. Based on these results, the total and irreversible fouling (R_{ir}) in the modified membranes has significantly improved compared to the unmodified membrane, which has confirmed the anti-fouling properties of the modified membranes. According to the rules of fouling, hydrophilicity and protrusion of the membrane surface are the most important factors controlling the membrane so that, by increasing hydrophilicity the fouling phenomenon is also reduced. In modified membranes, the highest ratio of fouling is from reversible fouling, which can be eliminated at a much lower and simpler cost than irreversible fouling [34,39].

4. Performance of Synthesized Membranes in the Removal of Direct Red 16 Dye

To evaluate the effectiveness of synthesized polyether-sulfone membranes in dye removal, a solution with a concentration of 50 ppm from Direct Red 16 was first prepared. Then after passing this solution over the membrane and measuring the absorption rate of the output solution from the membrane at the wavelength λ_{max}= 526.6 nm and comparing it with the absorption rate of the initial dye solution, the amount of membrane dye removal was calculated. The diagram of dye removal of modified membranes with different weight percentages of nanoparticles is given in Fig. 8(a). As the results show, the membrane containing 0.5 wt% of functionalized nanocrystals shows the highest amount of dye removal among the fabricated membranes. This feature can be related to the specific morphology of the membrane as well as the ability to absorb dye by functionalized nanocrystals on the surface and inside the membrane cavities [40]. Fig. 8(b) shows the dye permeation flux through fabricated membranes with different percentages of functionalized nanocrystals. As shown in Fig. 8(b), the flux of nanoparticle-modified membranes in dye filtration is higher than that of pure membranes, which can be attributed to the increase in surface hydrophilicity due to the addition of functionalized nanocrystals.

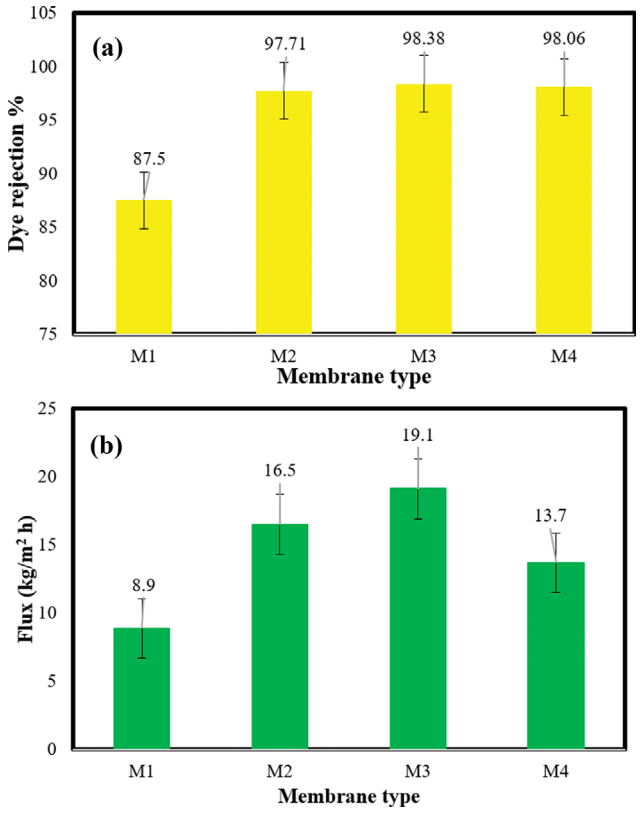

Fig. 8. (a) Performance of fabricated membrane in dye removal, (b) permeation flux of dye through fabricated membrane for modified membranes with different weight percentages of CNF-AAC.

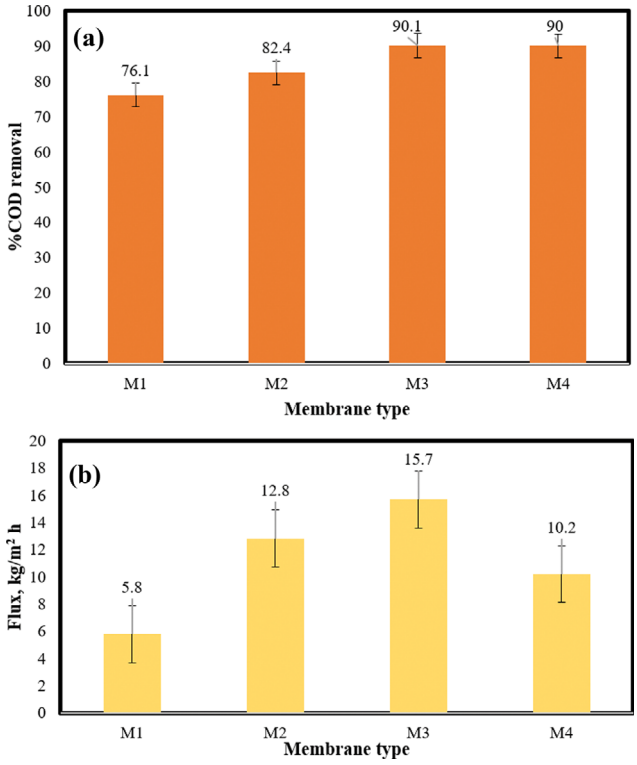

Fig. 9. (a) Fabricated membranes performance in COD removal from wastewater of licorice extract factory, (b) Permeation Flux wastewater of modified membranes with different weight percentages of CNF-AAC.

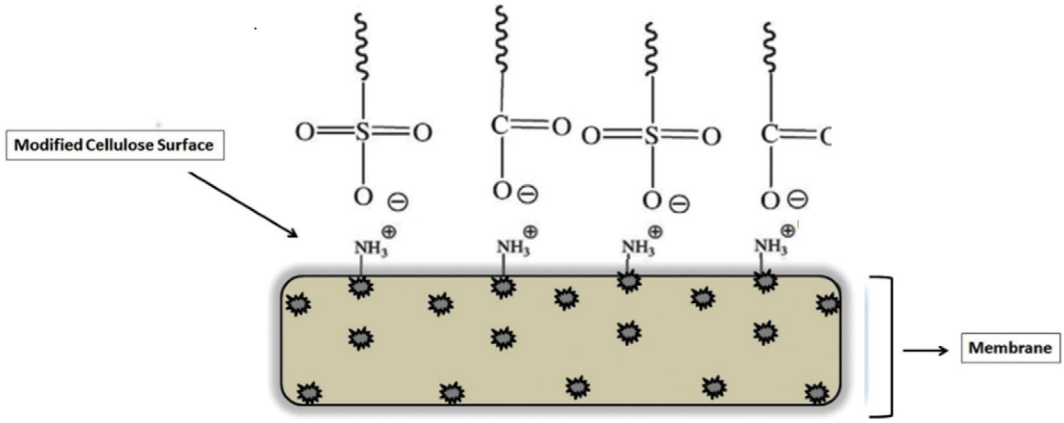

Fig. 10. The electrostatic attraction between the anionic groups of the colored dissolved compounds and cationic groups (-NH^{3+}) of modified adsorbent.

5. Performance of Synthesized Membranes in Wastewater Treatment of LEP Wastewater

Fig. 9(a) shows the COD removal rate from the wastewater using fabricated membranes. According to Fig. 9(a), the highest amount of COD removal is related to the membrane with 0.5% of functionalized nanocrystals. However, the COD removal rate in modified membranes is higher than pure polyether-sulfone membranes.

Fig. 9(b) shows the wastewater permeation flux through membranes fabricated with different percentages of functionalized nanocrystals. As shown in Fig. 9(b), due to the increase in membrane surface hydrophilicity, the reduction of membrane fouling and the smoothing of the membrane surface due to the addition of functionalized nanocrystals, the permeation flux of the modified membranes with functionalized nanocrystals is higher than pure membrane. Due to the existence of different functional groups on the surface of the used membrane and also their specific properties such as specific surface area, and high porosity, the COD and dye reduction mechanism could be mainly based on the attraction between pollutants and adsorbent by electrostatic attraction and hydrogen bonding, which are schematically shown in Fig. 10. It is clear that due to the presence of anionic sulfate ester groups at the surface of cellulose nanocrystals, their surface has an anionic charge. After modification of the cellulose nanocrystals with AAC, amine functional groups are also added to the adsorbent. In acidic conditions, the amount of dye reduction is increased by the electrostatic attraction between the anionic groups of the colored dissolved compounds and cationic groups (-NH^{3+}) of the modified adsorbent. In addition, another type of adsorption mechanism that can be expressed for this phenomenon is the formation of hydrogen bonding between hydroxyl groups of cellulose surfaces and different groups of colored dissolved compounds [41]. However, the permeation flux rate through the membrane for the wastewater of the LEP is less than Direct Red 16 dye, which is due to the high diversity of organic materials that increases the fouling of the membrane in the treatment of this wastewater.

CONCLUSION

Hydrophilic membranes with high anti-fouling capability were used to remove dye (Direct red 16) and to treat the wastewater of the LEP. Modified membranes had higher anti-fouling properties and higher flux than pure polyether-sulfone membranes. One of the problems of the membrane was its fouling, which reduced its lifespan and output flux. The use of hydrophilic functionalized nanocrystals increased the hydrophilicity feature of the synthesized membrane and on the other hand reduced the adhesion of organic materials to the membrane surface. Also, the addition of functionalized nanocrystals led to increase in the porosity and the water permeation flux rate through the fabricated membranes. Nanofiltration membranes that have so far been used to remove dyes and organic pollutants are based on molecular sieves and have a relatively low flux. In this work, CNF-AAC was used to modify membranes and results showed excellent performance in removal of dyes and organic pollutants. In this regard, the addition of CNF-AAC greatly increased the permeation flux through the membrane compared to the pure polyether-sulfone membrane and increased the membrane resistance to fouling, which is due to the change in volume structure of the membrane and increase in hydrophilicity of the membrane surface. On the other hand, by increasing the concentration of CNF-AAC (from 0.5 wt% to 1 wt%), the hydrophilicity of the membrane surface increased. However, by increasing the concentration of CNF-AAC (from 0.5 wt% to 1 wt%), the hydrophilicity of the membrane surface increased. But due to the adhesion of nanoparticles and the clogging of pores and creating a non-uniform surface for the membrane, the permeation flux rate through membrane, as well as its resistance to fouling, decreased. Therefore, the modified membrane with CNF-AAC 0.5 wt% was selected as the optimal membrane. According to FESEM images, it can be seen that the addition of CNF-AAC resulted in the formation of a membrane under layer with wider finger cavities and higher porosity than pure polyether-sulfone membranes. Also, the results of AFM analysis showed that the surface roughness of polyether-sulfone membrane is reduced by adding CNF-AAC. Surface roughness parameters for the modified membrane with 0.5 wt% of CNF-AAC had the lowest value; however, the surface roughness parameters in the modified membranes with weight percentages higher than 0.5 were higher than those of the polyether-sulfone membrane. Optimal membrane performance was evaluated in terms

of the ability to remove Direct red 16 dye and remove organic materials from the wastewater of the LEP. The optimum membrane permeation flux rate for removal of Direct Red 16 dye (19.1 kg/m^2h) was higher than the removal of organic materials from the wastewater of LEP (15.7 kg/m^2h), while removal percentage of dye and COD was 98.38% and 90.1%, respectively.

DECLARATION OF INTEREST

No funding was received to assist with the preparation of this manuscript.

The authors have no conflicts of interest to declare that are relevant to the content of this article.

REFERENCES

1. S. N. Hoseini, A. K. Pirzaman, M. A. Aroon and A. E. Pirbazari, *J. Water Process Eng.*, **17**, 124 (2017).
2. M. Arab Chamjangali, G. Bagherian, A. Javid, S. Boroumand and N. Farzaneh, *Spectrochim. Acta, Part A*, **150**, 230 (2015).
3. B. Zohra, K. Aicha, S. Fatima, B. Nourredine and D. Zoubir, *Chem. Eng. J.*, **136**, 295 (2008).
4. A. Pandey, P. Singh and L. Iyengar, *International Biodeterioration & Biodegradation*, **59**, 73 (2007).
5. P. Malik and S. Saha, *Sep. Purif. Technol.*, **31**, 241 (2003).
6. M. Koch, A. Yediler, D. Lienert, G. Insel and A. Kettrup, *Chemosphere*, **46**, 109 (2002).
7. T. Panswad and S. Wongchaisuwan, *Water Sci. Technol.*, **18**, 139 (1986).
8. M. Kamari, S. Shafiee, F. Salimi and C. Karami, *Desalin. Water Treat.*, **161**, 304 (2019).
9. F. Salimi, H. Rahimi and C. Karami, *Desalin. Water Treat.*, **137**, 334 (2019).
10. G. Busca, S. Berardinelli, C. Resini and L. Arrighi, *J. Hazard. Mater.*, **160**, 265 (2008).
11. R. O. Dunn Jr., J. F. Scamehorn and S. D. Christian, *Sep. Sci. Technol.*, **20**, 257 (1985).
12. J. Siemiatycki, L. Richardson, K. Straif, B. Latreille, R. Lakhani, S. Campbell, M.-C. Rousseau and P. Boffetta, *Environ. Health Perspect.*, **112**, 1447 (2004).
13. C. Conidi, L. Fuc, E. Drioli and A. Cassano, *Molecules*, **24**, 2279 (2019).
14. R. Mukherjee and S. De, *J. Hazard. Mater.*, **265**, 8 (2014).
15. R. Mukherjee and S. De, *Chem. Eng. J.*, **302**, 773 (2016).
16. R. W. Baker, *Membrane technology and applications*, John Wiley & Sons (2012).
17. S. Madaeni, M. Sohrabi, M. Khosravi and A. Ghaedi, *Sep. Sci. Technol.*, **46**, 1406 (2011).
18. L. J. Gorgol, S. G. Taub and J. Olesiewicz, U.S. Patent, US20110196138A1 (2011).
19. M. Jonoobi, A. Ashori and V. Siracusa, *Polymer Testing*, **76**, 333 (2019).
20. F. Rafieian, M. Hosseini, M. Jonoobi and Q. Yu, *Cellulose*, **25**, 4695 (2018).
21. S. Norouzbahari, R. Roostaazad and M. Hesampour, *Desalination*, **238**, 174 (2009).
22. R. E. Abouzeid, R. Khiari, N. El-Wakil and A. Dufresne, *Biomacromolecules*, **20**, 573 (2018).
23. F. Rafieian, M. Jonoobi and Q. Yu, *Cellulose*, **26**, 3359 (2019).
24. L. A. Goetz, N. Naseri, S. S. Nair, Z. Karim and A. P. Mathew, *Cellulose*, **25**, 3011 (2018).
25. H. Bai, X. Wang, Y. Zhou and L. Zhang, *Prog. Nat. Sci.: Mater. Int.*, **22**, 250 (2012).
26. Z. Jahan, M. B. K. Niazi and Ø. W. Gregersen, *J. Ind. Eng. Chem.*, **57**, 113 (2018).
27. S. Zinadini, A. A. Zinatizadeh, M. Rahimi, V. Vatanpour and H. Zangeneh, *J. Membr. Sci.*, **453**, 292 (2014).
28. E. Bagheripour, A. Moghadassi, S. Hosseini and M. Nemati, *J. Membr. Sci. Res.*, **2**, 14 (2016).
29. V. Vatanpour, S. S. Madaeni, A. R. Khataee, E. Salehi, S. Zinadini and H. A. Monfared, *Desalination*, **292**, 19 (2012).
30. R. P. Cossee, E. R. Geus and E. J. Van U.S. Patent, 6,488,856 (2002).
31. S. Hokkanen, A. Bhatnagar and M. Sillanpää, *Water Res.*, **91**, 156 (2016).
32. M. T. Koschevic, M. dos Santos, R. C. de Faria, F. M. Fakhouri and S. M. Martelli, *Chapter 9 - cellulose nanocrystals functionalization by grafting*, V. K. Thakur Ed., Biopolymer Grafting, Elsevier, 409 (2018).
33. M. R. K. Sofla, R. Brown, T. Tsuzuki and T. Rainey, *Adv. Nat. Sci.: Nanosci. Nanotechnol.*, **7**, 035004 (2016).
34. Q. Cheng, D. Ye, C. Chang and L. Zhang, *J. Membr. Sci.*, **525**, 1 (2017).
35. S. Zinadini, S. Rostami, V. Vatanpour and E. Jalilian, *J. Membr. Sci.*, **529**, 133 (2017).
36. V. Vatanpour, S. S. Madaeni, R. Moradian, S. Zinadini and B. Astinchap, *J. Membr. Sci.*, **375**, 284 (2011).
37. E. Celik, H. Park, H. Choi and H. Choi, *Water Res.*, **45**, 274 (2011).
38. J. Barzin, C. Feng, K. C. Khulbe, T. Matsuura, S. S. Madaeni and H. Mirzadeh, *J. Membr. Sci.*, **237**, 77 (2004).
39. J. Lv, G. Zhang, H. Zhang, C. Zhao and F. Yang, *Appl. Surf. Sci.*, **440**, 1091 (2018).
40. Z. Karim, A. P. Mathew, M. Grahn, J. Mouzon and K. Oksman, *Carbohydr. Polym.*, **112**, 668 (2014).
41. M. Rahimi, S. Dadari, S. Zeinaddini and E. Mohamadian, *Korean J. Chem. Eng.*, **34**, 1444 (2017).